Complex Waste Stream Utilization for Hydrogen Evolution: Ammonia Borane Hydrolysis Over Red Mud Catalyst Under Mild Conditions

Catalysis Letters (2025) 155:273
https://doi.org/10.1007/s10562-025-05112-7

Complex Waste Stream Utilization for Hydrogen Evolution: Ammonia Borane Hydrolysis Over Red Mud Catalyst Under Mild Conditions

Mattia Bartoli[1,2] · Marco Etzi[1] · Stefania Lettieri[3] · Giuseppe Ferraro[3] · Candido Fabrizio Pirri[1,3] · Angelica Monica Chiodoni[1] · Sergio Bocchini[1,2,3]

Received: 12 May 2025 / Accepted: 1 July 2025

Abstract
The utilization of red mud is a topic of significant interest due to its great production around the world, being the major by-product of alumina production. Nevertheless, its correct valorization is a matter of great complexity. In this work, we propose a novel use of red mud as a catalyst for the release of hydrogen from hydrolysis of ammonia borane in mild conditions. Ammonia borane is among the best chemical hydrogen carriers with a gravimetric hydrogen capability of up to 19 wt% but is characterized by a complex reactivity under thermal stimuli. Accordingly, ammonia borane hydrolysis has emerged as a solid route for direct and safe hydrogen release. In this work, we achieved complete hydrolysis of ammonia borane both at 30 °C and 40 °C after 660 s and 12 s, respectively, with a red mud loading of 10 wt%. The addition of red mud decreased the activation energy of the hydrolysis reaction over 90% and increased the kinetic constant over two orders of magnitude. Furthermore, red mud preserved the catalytic activity after three cycles with no significant changes.

Keywords Ammonia borane · Hydrogen storage · Red mud · Hydrogen evolution · Hydrolysis

1 Introduction

Nowadays, energy demand has considerably depleted the available resources compromising the quality of both health and environment [1]. Several complex waste streams retain a great value in resources even if their efficient utilization is quite complex [2, 3]. Among them, the solid waste residue resulting from the alkaline digestion of bauxite ores known as red mud (RM) is of particular interest due to its composition rich in alumina, silica, iron oxide, and titania [4, 5]. The disposal of RM is quite complex due to its diverse composition and the amount produced (around 600 Mton in 2019 [6]). RM disposal is also expensive and represents up to 2% of the final cost of alumina. Accordingly, the efforts of both the academic and industrial communities have been devoted to the valorization of RM with the minimum amount of efforts due to its relatively stable composition considering its major components [7]. Venkatesh et al. [8] diffusely described the utilization of RM as an additive for the production of reinforced cement, while other authors proposed the use of RM as a composite filler [9–11] or as a catalyst [12–14]. Particularly, Das et al. [15] suggested the utilization of RM-based catalysts for the green energy transition in the thermal cracking of several feedstocks. Interestingly, RM catalyst can be efficiently used for the production of molecular hydrogen, as reported by Kurtoğlu et al. [16]. The authors used an RM-derived catalyst for the release of molecular hydrogen from the decomposition of ammonia while other studies reported similar processes using methane [17]. Hydrogen release from molecular stable precursors is a promising solution for achieving a carbon-negative society based on hydrogen-fuelled technologies [18, 19]. Among safe hydrogen storage precursors, ammonia borane (AB) stands as one with the highest gravimetric capacity up to 19.6 wt%. Nevertheless, AB complex thermal reactivity [20] prevents its use for the release of molecular hydrogen

✉ Mattia Bartoli
mattia.bartoli@iit.it

1 Center for Sustainable Future Technologies—CSFT@POLITO, Istituto Italiano di Tecnologia, Via Livorno 60, Torino 10144, Italy

2 Consorzio Interuniversitario Nazionale per la Scienza e Tecnologia dei Materiali (INSTM), Via G. Giusti 9, Florence 50121, Italy

3 Department of Applied Science and Technology, Politecnico di Torino, C.so Duca degli Abruzzi 24, Turin 10129, Italy

Published online: 12 July 2025

under thermal stimuli [20]. Alternatively, AB hydrolysis represents a simple and solid alternative route for the release of hydrogen in presence of water using several types of catalytic materials [21], including ionic liquids [22–24], carbon [25] or inorganic porous species [26–28], and nanostructured metal supported catalysts [29–34]. Actually, the most performing catalyst contains costly supports (i.e. carbon nanotubes [35], graphene oxide [36]) and contains critical raw metals such as platinum group metals [37–41].

In this work, we investigated the utilization of RM as catalysts for AB hydrolysis under mild conditions to merge the virtuous management of RM with the challenging field of chemical hydrogen storage and release. We investigate the use of RM as an efficient, low-cost catalyst for the hydrolysis of AB under mild conditions valorizing an industrial waste while enabling high hydrolytic conversion of AB with release of hydrogen. Contrary to conventional catalysts based on scarce or expensive metals, RM provides an abundant alternative with inherent catalytic activity due to its composition, particularly iron, aluminum, and titanium oxides. Furthermore, RM exhibits excellent stability and reusability over multiple cycles, reinforcing its potential for scalable applications. This work stands out by merging waste remediation with clean energy production promoting a virtuous approach to hydrogen storage and release.

2 Materials and Methods

2.1 Materials

Sodium Borohydride (>99%), Ammonium sulfate (>98%), and tetrahydrofuran (THF, >98) were purchased from Merck-Sigma Aldrich and they were used without any additional purification.

RM was provided by Alcan International Ltd., Canada as slurry, dried in a muffle oven at 105 ºC for 12 h and then pulverized manually.

2.2 Synthesis of AB

AB was synthesized and purified accordingly with an experimental procedure reported by Ramachandran et al. [42]. $NaBH_4$ (3.25 g, 0.086 mol, 1 eq.) was dissolved in 150 mL of THF and $(NH_4)_2SO_4$ (13.21 g, 0.100 mol, 1.1 eq.) and the reaction mixture was stirred at 40 °C for 6 h. The reaction mixture was cooled down and filtered to remove the Na_2SO_4 formed and the solution was dried to recover AB as a white solid, which was further dried under vacuum at 40 °C overnight. AB was used without any further purification. AB was analyzed in order to evaluate the presence of contaminants and no other species were detected.

2.3 Materials Characterization

RM was characterized using Raman spectroscopy (Renishaw inVia (H43662 model, Gloucestershire, UK) equipped with a red laser line source (785 nm) in the range from 200 to 1000 cm^{-1}.

RM were analyzed through Fourier transform infrared (FT-IR) (ATR mode) spectroscopy using a TENSOR II spectrometer (Bruker) equipped with a ATR module Platinum II (Bruker).

The specific surface area of RM was measured using N_2 sorption at −196 °C by using a Micromeritics Tristar II (Micromeritics Instrument Corporation, USA) and applying the Langmuir model.

XRD patterns were acquired by using a Panalytical diffractometer (X'PERT PRO PW3040/60 Almelo, The Netherlands). with a Cu K α radiation at 40 kV and 40 mA as X-Ray source. The diffraction patterns were obtained from RM powder in the 2θ range from 20º to 80° (step size of 0.013°) and analyzed by using QualX software.

RM was investigated by using X-ray photoelectron spectroscopy (XPS) using a PHI 5000 VersaProbe Physical Electronics (Chanhassen, MN, USA) scanning X-ray photoelectron spectrometer (monochromatic Al K-alpha X-ray source with 1486.6 eV energy, 15 kV voltage, and 1 mA anode current).

The elemental composition and morphology of RM particles were investigated using a Field Emission Scanning Electrical microscope (FE-SEM, Zeiss SupraTM 25 Oberkochen, Germany) operating at 5 keV equipped with an energy dispersive X-ray detector (EDX, Oxford Inca Energy 450, Oberkochen, Germany) operating at 10 keV.

2.4 AB Hydrolytic Test for Hydrogen Evolution

AB hydrolysis was carried out at different temperatures (20, 30, and 40 °C) in a nitrogen atmosphere using a procedure established by Gianola et al. [43]. RM was placed in a two-neck flask connected to a gas burette and to a pressure-equalized funnel as reported in Scheme 1.

RM was stirred at 300 rpm for 10 min and AB was added reaching a final concentration of 0.5 M and an RM/AB ratio of 0, 5, and 10.0 wt%. The hydrogen evolution was monitored using the gas burette considering the external pressure and temperature. After the catalytic test, the catalyst was recovered by filtration, dried under vacuum (20 mbar, 50 °C). Each catalytic test was replicated three times and no detectable changes were observed among them.

Conversion was calculated as follow:

$$Conversion : 100 * \frac{n_{H_2\,produced}}{n_{H_2\,AB}}, \quad (1)$$

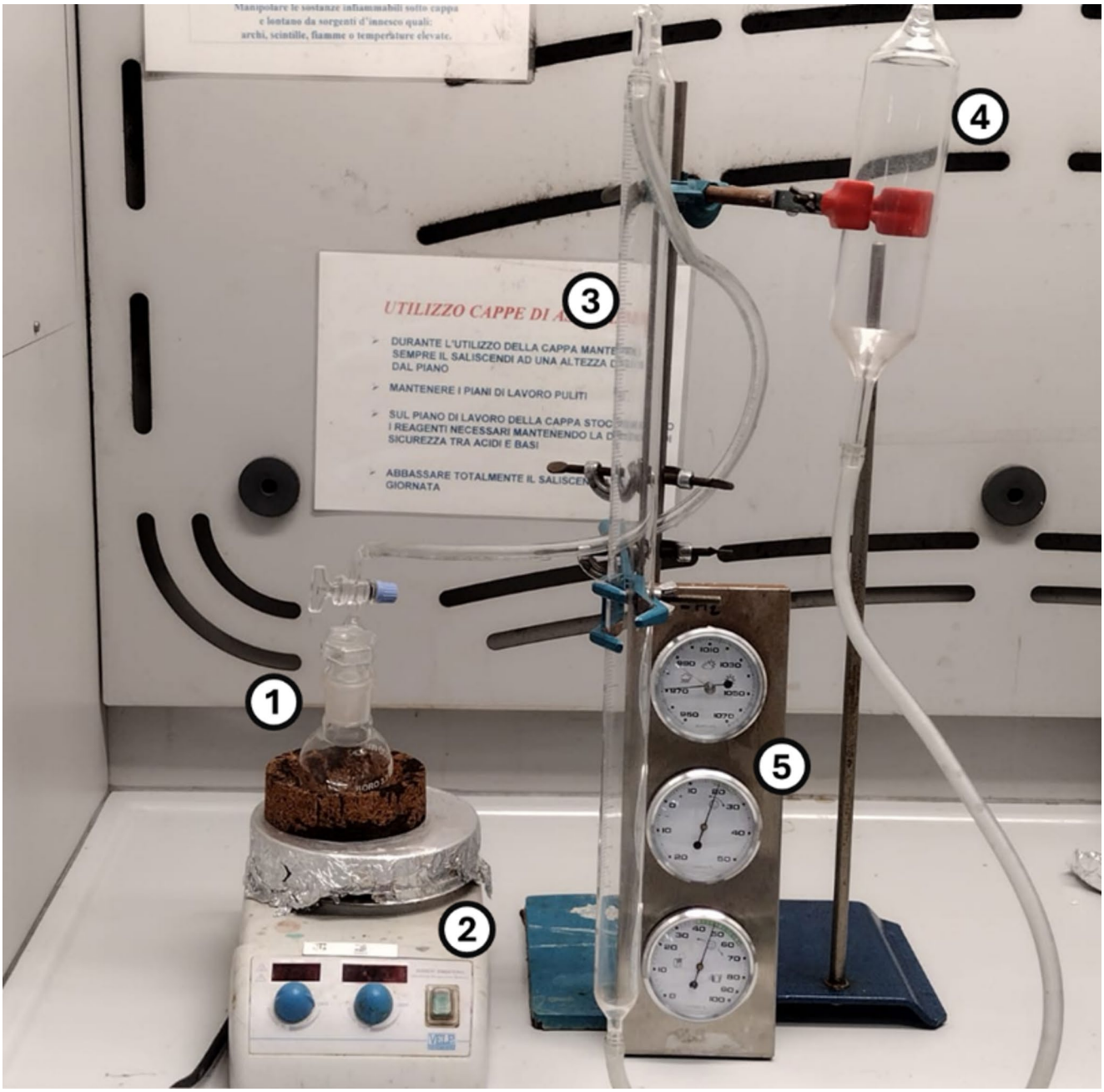

Scheme 1 Set up for monitoring gas evolution: (1) heater, (2) reaction vessel, (3) volumetric burette, (4) expansion chamber and (5) barometric station

$$n_{H_{2produced}} = \frac{P * V}{R * T}, \tag{2}$$

$$\ln(k) = \ln(a) + \frac{\Delta E_a}{RT}, \tag{3}$$

where P is the measured atmospheric pressure, V is the volume of hydrogen released, T is the temperature and R is the molar gas constant.

Kinetic constants (k) for each reaction were obtained by using a pseudo first order model as reported by Abutaleb et al. [44] and activation energies (ΔE_a) were calculated by using the Arrhenius equation [45] reported as follows:

where k is a rate constant, a is a pre-exponential factor, R is the gas constant, and T is the reaction temperature measured in K.

3 Results and Discussion

3.1 Characterization of the Catalysts

The materials were initially characterized by XRD, IR and Raman spectroscopy (Fig. 1).

As reported in Fig. 1a, the XRD pattern of neat RM (black curve) shows the simultaneous presence of silica, iron oxide, alumina, and sodium oxide, with traces of titanium oxide, in accordance with the current knowledge of RM composition [46]. Raman spectrum of this sample (Fig. 1b, black curve) supports the presence of such species with signal centered at 222 and 292 cm^{-1}, 405 cm^{-1} and 610 cm^{-1} due to the vibrational mode Fe-O, Si-O and Al-O, respectively [47]. As reported in Fig. 1c, FT-IR spectra showed the n_{Si-O} centered at 997 cm^{-1} [48] and the n_{Fe-O} [49] centered at 429 cm^{-1} prior and after three catalytic cycles without observing any residual species from AB hydrolysis [20]. There are no evidence of residual organic contaminants from the recovery process of RM suggesting that the procedure enforced for recovery it guaranteed good reproducibility despite the collecting period [4]. The morphological analysis of RM (Fig. 2a) showed the presence of micrometric flower-like particles with a specific surface area of up to 8.3 m^2 g^{-1} and a pore volume of up to 0.06 cm^3/g. The elemental composition reported in Table 1 showed a significant amount of iron and aluminum up to 30.2 and 13.5 wt% respectively. Such a large amount of these elements is critical for the utilization of RM as a catalyst for AB hydrolysis as mentioned by several authors [50, 51]. On the other hand, the presence of Ti (5.1 wt%) and Na (4.3 wt%) can be highly beneficial for the RM catalytic activity in the hydrolysis of AB as reported by Kalindi et al. [52].

As reported in Fig. 3a, the iron contained into RM was Fe(III) with a two peaks (2 p 3/2 and 1/2) centred at 711.0 and 724.6 eV respectively and two satellite peaks at 715.4 and 732.4 eV. The signal of Al 2p showed only a one peak due to Al(III) centered at 73.5 eV. The oxidation states of

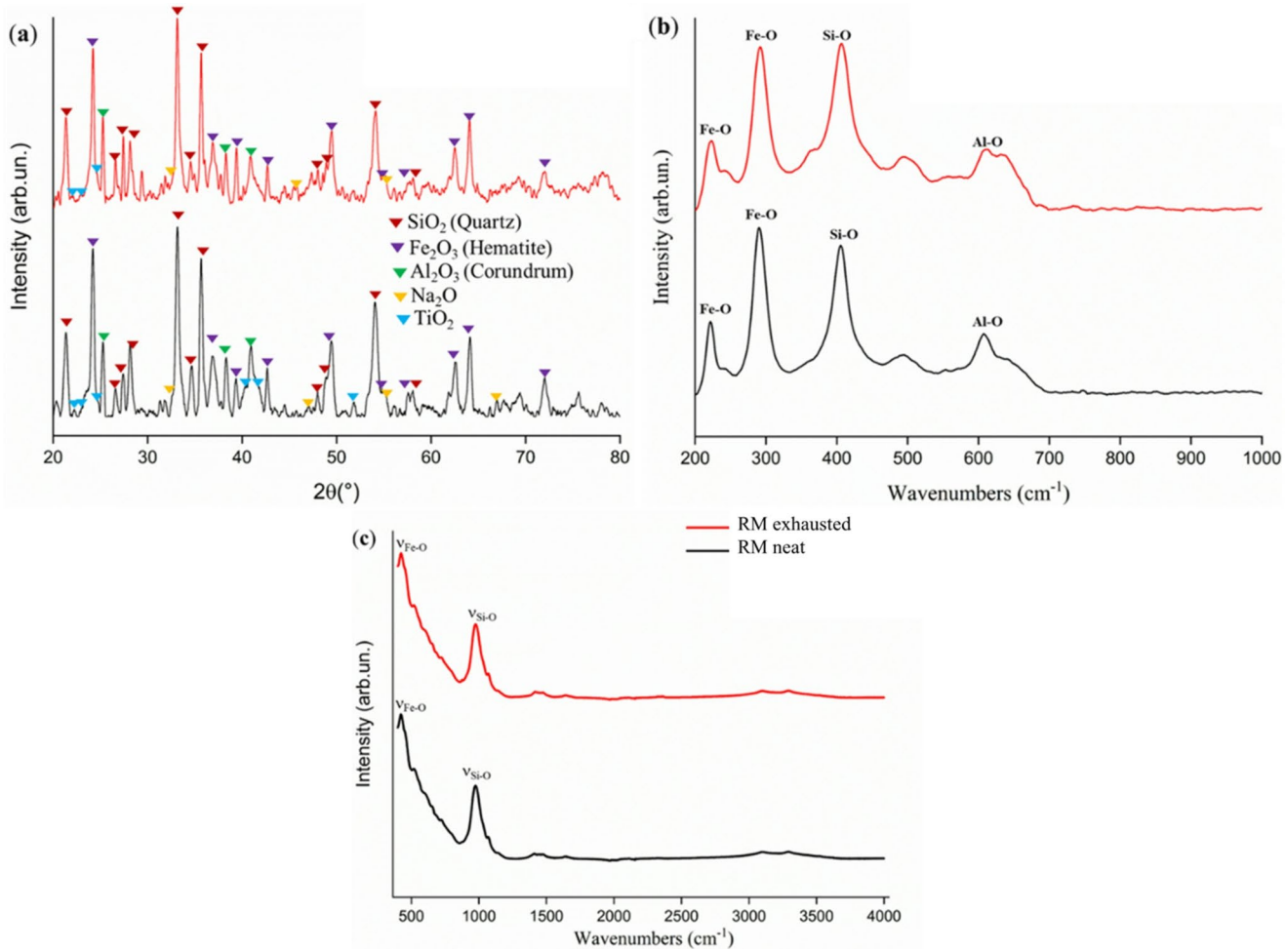

Fig. 1 Investigation of the crystalline structure of RM prior (black lines) and after five catalytic cycles (red lines) using (**a**) XRD in the 2q range from 20º up to 80º and (**b**) Raman spectra of RM before and after three catalytic cycles in the region from 200 to 1000 cm^{-1} and (**c**) FT-IR (ATR mode) spectra of RM before and after three catalytic cycles in the region from 500 to 4000 cm^{-1}

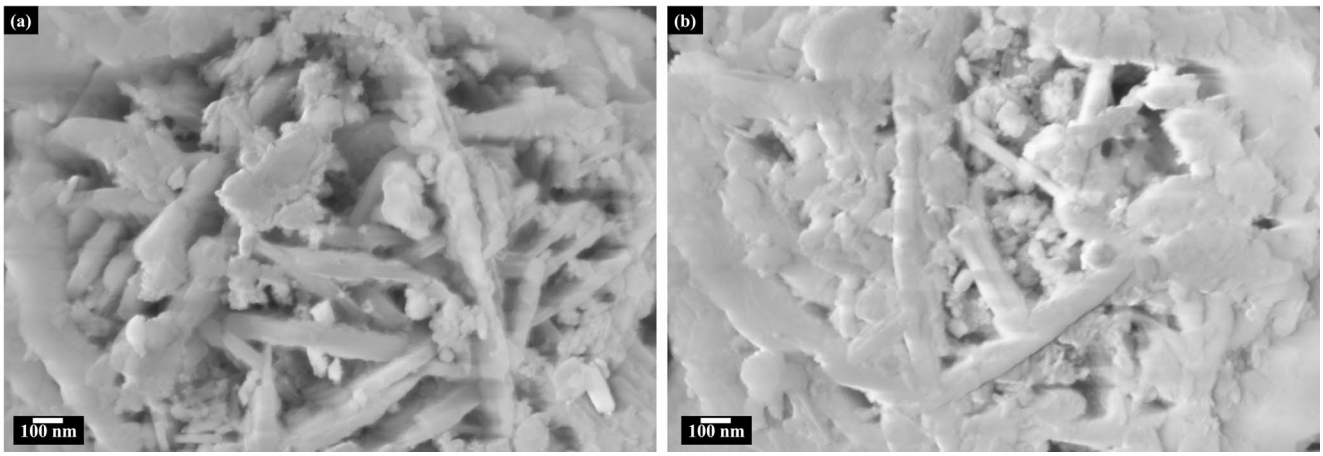

Fig. 2 FE-SEM images of RM (**a**) before and (**b**) after five catalytic cycles

Table 1 Chemical composition evaluated through EDX analysis of RM before and after five catalytic cycles

Element	RM (wt%)	
	Neat	After five catalytic cycles
O	41.2	39.3
Na	4.3	4.5
Al	13.5	13.2
Si	5.7	5.1
Ti	5.1	5.2
Fe	30.2	32.7

both iron and aluminum were in good agreement with the XRD data and the presence of their oxides.

3.2 Catalytic Tests

The AB hydrolysis mechanism is summarized in Fig. 4 showing a selective production of molecules of H_2 for each unit of AB reacted with water and the formation of adsorbed boron species [53] on M(III) sites. As reported by Lapin et al. [51], the acidic sites of metal are able to drastically increase the hydrolytic kinetics of AB hydrolysis while the other oxides (i.e.silica, titania, and sodium oxide) can further boost this reactivity through adsorption processes as reported by several authors [54–56].

The simultaneous presence of both Fe(III) and Al(III) as shown by Fig. 3 and b support the acid sites mediated mechanism of RM while the XRD spectrum (Fig. 1a) confirmed the presence of complex support of mixed and poorly crystalline oxide.

We evaluated the hydrogen release from AB hydrolysis process at temperatures from 20 °C to 40 °C using a RM loading ranging of 0, 5 and 10 wt%, as reported in Fig. 5, evaluating both ΔE_a and k as reported in Table 2).

As reported in Fig. 5a, the non-catalyzed hydrolysis of AB involves a very slow and poor release of hydrogen, reaching a maximum conversion of 21.2% at 20 °C after 900 s according with the literature [57]. A moderate increment was observed by increasing the temperature up to 40 °C with a conversion of 32.3%, while a comparable conversion to that obtained at 20 °C was observed at 30 °C (24.8%). The increase in reaction temperature slightly affected k, that reached a value of $9.0 \cdot 10^{-3}$ s^{-1} at 40 °C.

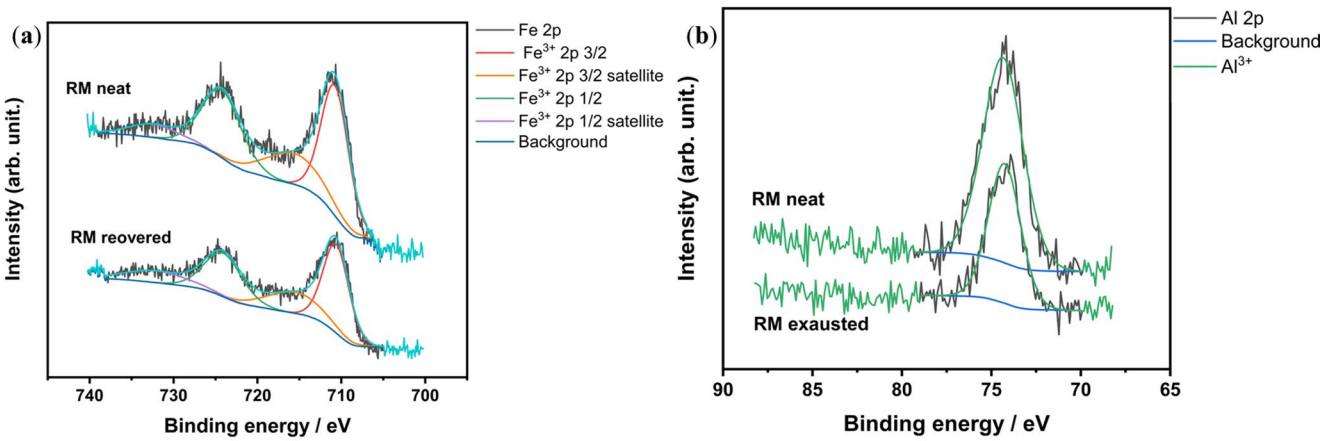

Fig. 3 XPS spectra of (**a**) Fe and (**b**) Al of RM (**a**) before and (**b**) after five catalytic cycles

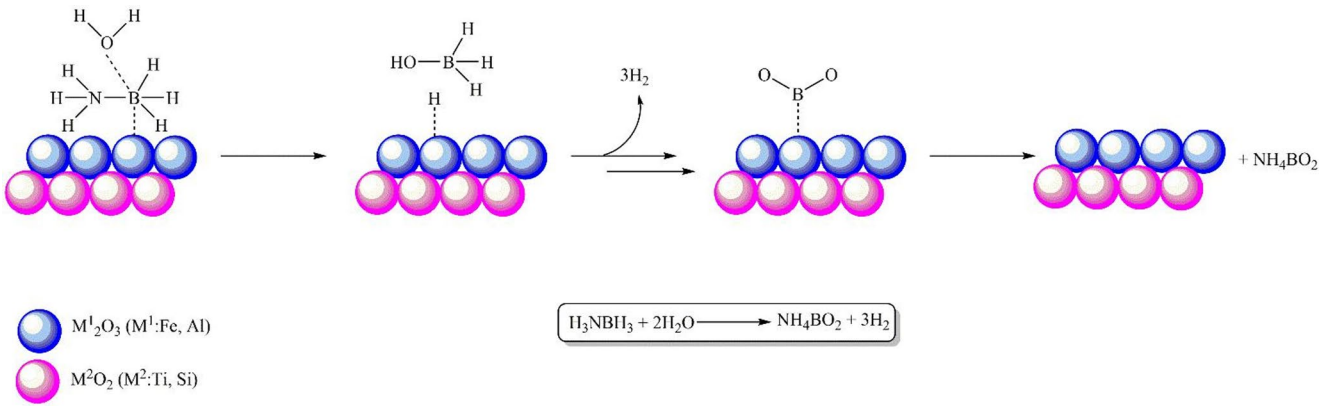

Fig. 4 Hypothetical mechanism of AB hydrolysis over multimetallic RM catalyst

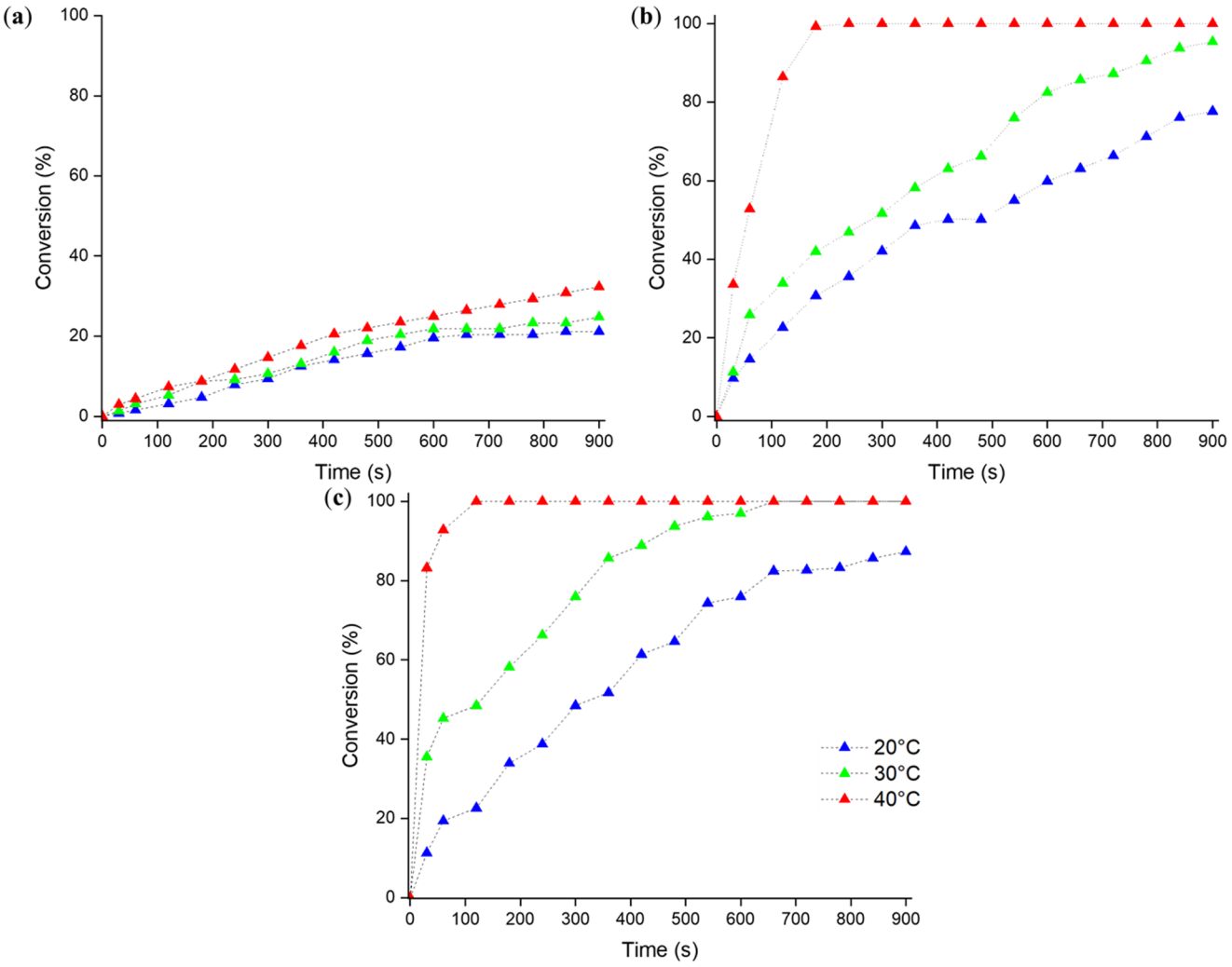

Fig. 5 Hydrogen release experiments carried out using a loading of RM of (**a**) 0 wt%, (**b**) 5 wt%, and (**c**) 10 wt%

As shown in Fig. 5b, the addition of RM with a loading of up to 5 wt% improved the hydrogen release reaching total conversion after 240 s at 40 °C, with an increase in k from $2.0 \cdot 10^{-3}$ s^{-1} (20 °C) to $14.0 \cdot 10^{-3}$ (40 °C). These values are 10 times higher than those obtained for the non-catalyzed reaction. A further increase in RM loading up to 10 wt% (Fig. 5c) further improved the activity, with this sample reaching a total conversion at 30 °C after 660 s with a k of

Table 2 Values of ΔE_a and k of hydrolysis of AB under different loading of RM

RM loading (wt%)	k (s^{-1})			ΔE_a (kJ mol^{-1})
	20 °C	30 °C	40 °C	
0	0.6×10^{-3}	0.7×10^{-3}	0.9×10^{-3}	127
5	2×10^{-3}	3×10^{-3}	14×10^{-3}	73
10	2×10^{-3}	6×10^{-3}	57×10^{-3}	19

up to $3.0 \cdot 10^{-3}$ s^{-1}. A higher temperature further increased the reaction rate, reaching a total conversion after only 120 s with a k of up to $57.0 \cdot 10^{-3}$ s^{-1}. The influence of reaction temperature was further investigated by calculating the activation energy (ΔE_a) using k and Arrhenius equation. The positive effect of the catalyst was proved by the decrease of ΔE_a from 127 kJ mol^{-1} for the uncatalyzed reaction down to 19 kJ mol^{-1} using an RM loading of 10 wt%. Considering the decrement of ΔE_a, a close relation of between temperature and the formation of transitional state of adsorbed AB on the RM surface as reported by Wang et al. [58].

Next, we evaluated the stability of RM as catalyst: as shown in Fig. 6, all the samples (with different loadings) showed good stability upon 5 cycles at 40 °C, with only a small decrease in the reaction rate. Nevertheless, the catalytic system reached full conversion after 180 s. As reported in Fig. 1a, b (red curves), the XRD and Raman spectra did not show any significant modification while the elemental composition (Table 2) showed minor fluctuations, reasonably due to the small surface rearrangement while surface area remained similar (7.1 m^2 g^{-1}). As reported in Fig. 3a, b, the iron and aluminum preserved their oxidation states as Fe(III) and Al (III) after. This evidence support the stability of metal centres without any reduction induced by the presence of AB [59].

As reported in Fig. 1c (red curve), there were no absorbed residual species on the surface of the RM catalyst supporting

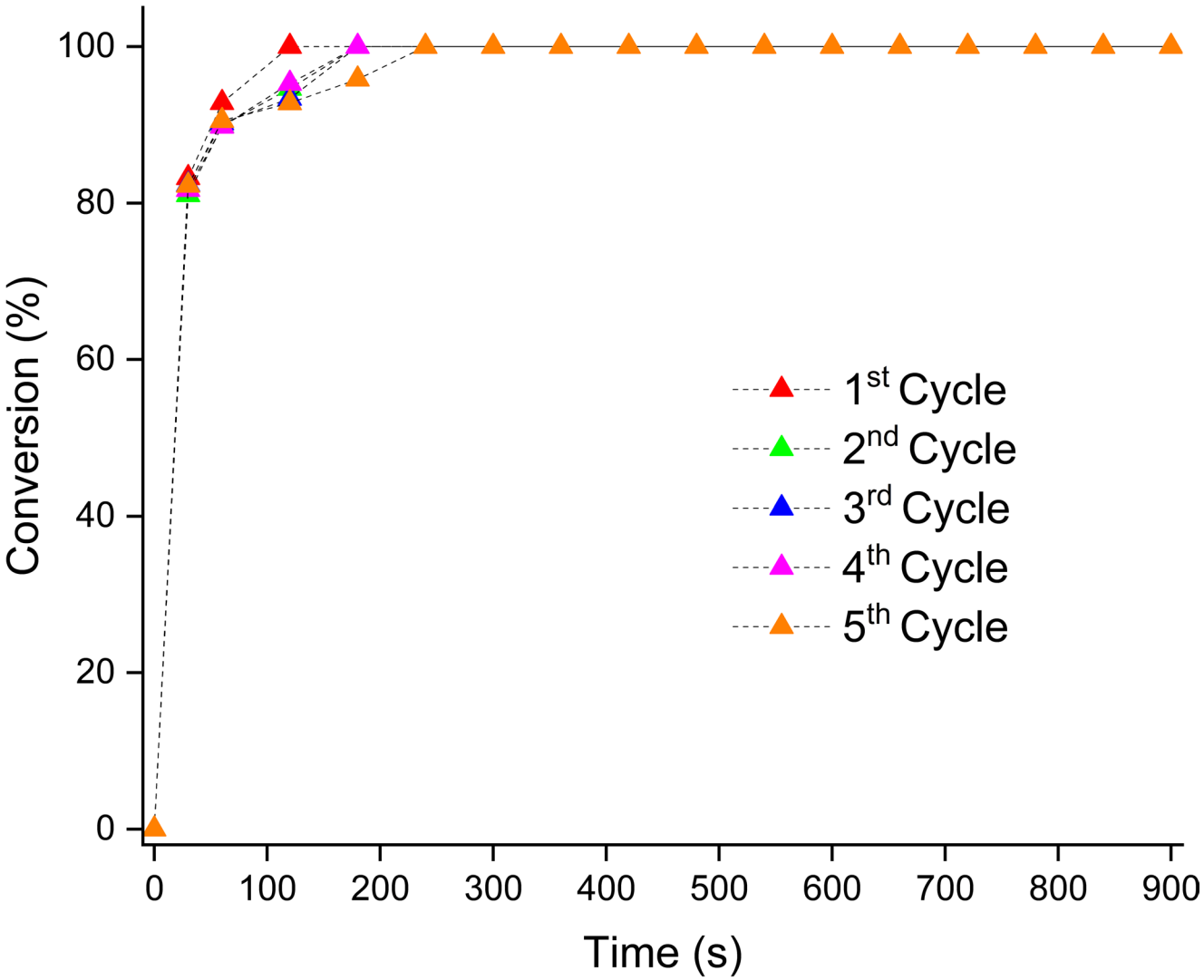

Fig. 6 Hydrogen evolution test with an RM loading up to 10 wt% during five catalytic cycles run at 40 °C

Table 3 Literature review and comparison of catalytic performance of RM and other performing catalysts

Catalyst	Particle size (nm)	Conversion (%)	t (min)	ΔE_a (kJ mol^{-1})	Catalyst loading (wt%)	Refs.
RM	> 100 nm	100	2	19	10	This work
Fe onto biochar	80	99	15	54	10	[43]
Co/Al_2O_3	13	99	70	62	10	[62]
Fe nanoparticles	60	100	8	Not reported	12	[64]
Ni nanoparticles	< 19	100	6	Not reported	10	[63]
Cu supported onto zeolite	50	100	120	54	2	[61]
Ru/Al_2O_3	2	100	3	23	2	[60]
Rh/Al_2O_3	3	100	2	21	2	[60]
Pt/Al_2O_3	2	100	1	21	2	[60]
Ru/zeolite	1	100	8	67	0.5	[66]

also the efficiency of desorption of dehydrogenated AB after the hydrolytic conversion.

We further compared the catalytic performances of RM for AB hydrolysis with those found in the literature for the same reaction. As shown in Table 3, RM showed a ΔE_a comparable with the one achieved by using noble metals nanoparticles supported onto alumina [60], outperforming copper [61], cobalt [62], nickel [63], and other iron-based catalysts [43, 64]. The good catalytic performances of RM were possibly due to the strong M(III) sites able to act as acidic sites surrounded by a very basic environment due to the sodium oxide, silica, and titania [65].

4 Conclusion

The hydrogen release from AB hydrolysis has gained great interest in the context of a hydrogen-based economy. Utilizing RM as a catalyst to improve the hydrogen release rate combines the valorization of a hard-to-manage waste stream with the superior performance of RM, guaranteed by the massive presence of non-critical raw metals, such as iron and aluminum, mixed in a silica defective-based matrix. The catalytic performances were among the best in literature, reaching a total conversion after 660 s and 120 s at 30 °C and 40 °C, respectively, using an RM loading of 10 wt%. Furthermore, we observed a two-order of magnitude increase in k and a 90% reduction of ΔE_a compared with the non-catalyzed process.

We believe that the valorization of complex metal-based waste represents a valuable strategy to boost a hydrogen-based economy and to promote a carbon-negative society development.

Acknowledgements This study was carried out within the Agritech National Research Center and received funding from the European Union Next-GenerationEU (PIANO NAZIONALE DI RIPRESA E RESILIENZA (PNRR)– MISSIONE 4 COMPONENTE 2, INVESTIMENTO 1.4– D.D. 1032 17/06/2022, CN00000022). Furthermore, authors wish to thank European Union for the financial support through the Next Generation EU- Piano Nazionale Resistenza e Resilienza (PNRR) projects "Nord Ovest Digitale E Sostenibile-NODES" (PNRR, D.D. n.1054 23/06/2022) and NEST " Network for Energy Sustainable Transition-NEST"(PE0000021, D.D. n.341 15/03/2022) and PNRR Mission 4 "Education and Research"—Component 2 "From research to business"—Investment 3.1 "Fund for the realization of an integrated system of research and innovation infrastructures"—Call for tender No. n. 3264 of 28/12/2021 of Italian Ministry of Research funded by the European Union—NextGenerationEU—Project code: IR0000027, Concession Decree No. 128 of 21/06/2022 adopted by the Italian Ministry of Research, CUP: B33C22000710006, Project title: iENTRANCE. The authors also acknowledge Ministero dello Sviluppo Economico (MISE) and Ministero della Transizione Ecologica (MITE) for the financial support. This manuscript reflects only the authors' views and opinions, neither the European Union nor the European Commission can be considered responsible for them.

Author contributions Mattia Bartoli: Conceptualization, methodology, formal analysis, investigation, visualization, supervision, writing—original draft preparation, writing—review and editingMarco Etzi: Methodology, formal analysis, investigation, visualization, writing—original draft preparation, writing—review and editingStefania Lettieri: Methodology, formal analysis, investigation, visualization, writing—original draft preparation, writing—review and editingGiuseppe Ferraro: Methodology, formal analysis, investigation, visualization, writing—original draft preparation, writing—review and editingCandido Fabrizio Pirri: Conceptualization, writing—original draft preparation, supervision, project administration, funding acquisitionAngelica Monica Chiodoni: Conceptualization, writing—original draft preparation, supervision, project administration, funding acquisitionSergio Bocchini: Conceptualization, writing—original draft preparation, supervision, project administration, funding acquisition.

Funding Open access funding provided by Istituto Italiano di Tecnologia within the CRUI-CARE Agreement.

Data availability Data is provided within the manuscript or supplementary information files.

Declarations

Ethics approval and consent to participate Not applicable.

Competing interests The authors declare no competing interests.

References

1. Hainsch K, Löffler K, Burandt T, Auer H, del Granado PC, Pisciella P, Zwickl-Bernhard S (2022) Energy 239:122067
2. Lamah L, Degny B, Yable D, Haba C (2024) J Mater Environ Sci 15(3):427440
3. Zhou Y, Cui Y, Yang J, Chen L, Qi J, Zhang L, Zhang J, Huang Q, Zhou T, Zhao Y (2024) J Environ Manage 356:120608
4. Agrawal S, Dhawan N (2021) Miner Eng 171:107084
5. Khairul M, Zanganeh J, Moghtaderi B (2019) Resour Conserv Recycl 141:483–498
6. Wang L, Sun N, Tang H, Sun W (2019) Minerals 9:362
7. Antunes MLP, Couperthwaite SJ, da Conceicao FT, Costa de Jesus CP, Kiyohara PK, Coelho ACV, Frost RL (2012) Ind Eng Chem Res 51:775–779
8. Venkatesh C, Nerella R, Chand MSR (2020) J Korean Ceram Soc 57:167–174
9. Zecchi S, Ruscillo F, Cristoforo G, Bartoli M, Loebsack G, Kang K, Piatti E, Torsello D, Ghigo G, Gerbaldo R, Giorcelli M, Berruti F, Tagliaferro A (2023) Micromachines 14:429
10. Qaidi SM, Tayeh BA, Isleem HF, de Azevedo AR, Ahmed HU, Emad W (2022) Case Stud Constr Mater 16:e00994
11. Dani M, Borad J, Shukla R (2015) Int J Adv Res Sci Eng 4:216–225
12. Sushil S, Batra VS (2008) Appl Catal B 81:64–77
13. Wang Q, Pittman AS, Cao Y (2025) Chin J Chem Eng 77:195–202
14. Liu S, Liu J, Wang J, Liu Y, Yang B, Hong M, Yu S, Qiu G, Fang Y (2025) J Environ Manage 375:124356
15. Das B, Mohanty K (2019) Renewable Energy 143:1791–1811
16. Kurtoğlu SF, Uzun A (2016) Sci Rep 6:32279
17. Fang X, Liu Q, Li P, Li H, Li F, Huang G (2016) J Nanomater:6947636-6947644
18. Bairrão D, Soares J, Almeida J, Franco JF, Vale Z (2023) Energies 16:551
19. Lagioia G, Spinelli MP, Amicarelli V (2023) Int J Hydrog Energy 48:1304–1322
20. Bartoli M, Pirri CF, Bocchini S (2022) J Phys Chem C 126:7
21. Guan S, Yuan Z, Zhao S, Zhuang Z, Zhang H, Shen R, Fan Y, Li B, Wang D, Liu B (2024) Angewandte Chemie 136(33): e202408193
22. Ahluwalia R, Peng J, Hua T (2011) Int J Hydrog Energy 36:15689–15697
23. Nakagawa T, Burrell AK, Del Sesto RE, Janicke MT, Nekimken AL, Purdy GM, Paik B, Zhong R-Q, Semelsberger TA, Davis BL (2014) RSC Adv 4:21681–21687
24. Valero-Pedraza MJ, Martín-Cortés A, Navarrete A, Bermejo MD, Martín Á (2015) Energy 91:742–750
25. Sam DK, Cao Y (2024) Renewable Energy 237:121788
26. Balla Á, Nagyházi M, Turczel G, Solt HE, Mihályi MR, Hancsók J, Valyon J, Nagy T, Kéki S, Anastas PT (2022) New J Chem 46:16309–16316
27. Pei Y, Niu Y, Zhang W, Zhang Y, Ma J, Li Z (2022) Int J Hydrog Energy 47:2819–2831
28. Wen J, Tang S, Ding X, Yin Y, Song F, Yang X (2024) Energies 17:5712
29. Meng Y, Sun Q, Zhang T, Zhang J, Dong Z, Ma Y, Wu Z, Wang H, Bao X, Sun Q (2023) J Am Chem Soc 145:5486–5495
30. Gong B, Wu H, Sheng L, Zhang W, Wu X (2022) ACS Appl Mater Interfaces 14:13231–13239
31. Tang S, Xu L, Ding X, Lv Q, Qin H, Li A, Yang X, Han J, Song F (2025) Fuel 381:133424
32. Qin H, Tang S, Xu L, Li A, Lv Q, Dong J, Liu L, Ding X, Jiang N, Luo R (2025) J Colloid Interface Sci 697:137897
33. Qin H, Tang S, Xu L, Li A, Lv Q, Dong J, Liu L, Ding X, Pan X, Yang X (2025) J Alloys Compd 1010:177644
34. Liang J, Li H, Chen L, Ren M, Fakayode OA, Han J, Zhou C (2023) Ind Crops Prod 193:116214
35. Guo A, Hu L, Peng Y, Wang Y, Long Y, Fu J, Fan G (2022) Appl Surf Sci 579:152158
36. Feng K, Zhong J, Zhao B, Zhang H, Xu L, Sun X, Lee ST (2016) Angew Chem Int Ed 55:11950–11954
37. Barakat NA (2013) Mater Lett 106:229–232
38. Özkar S (2021) Dalton Trans 50:12349–12364
39. Sun D, Mazumder V, Metin O, Sun S (2011) ACS Nano 5:6458–6464
40. Ma H, Na C (2015) ACS Catal 5:1726–1735
41. Wang L, Li H, Zhang W, Zhao X, Qiu J, Li A, Zheng X, Hu Z, Si R, Zeng J (2017) Angew Chem Int Ed 56:4712–4718
42. Ramachandran PV, Gagare PD (2007) Inorg Chem 46:7810–7817
43. Gianola G, Bartoli M, Pirri CF, Bocchini S (2023) Int J Hydrog Energy 51:21–28
44. Abutaleb A, Zouli N, El-Halwany M, Ubaidullah M, Yousef A (2021) Int J Hydrog Energy 46:35248–35260
45. Mohajeri N, Ali T, Adebiyi O (2007) J Power Sources 167:482–485
46. Castaldi P, Silvetti M, Santona L, Enzo S, Melis P (2008) Clays Clay Miner 56:461–469
47. He D, Xiong Y, Wang L, Sun W, Liu R, Yue T (2020) Minerals 10:583
48. Bartoli M, Giorcelli M, Rosso C, Rovere M, Jagdale P, Tagliaferro A (2019) Appl Sci 9:13
49. Paredes-García V, Toledo N, Denardin J, Venegas-Yazigi D, Cruz C, Spodine E, Luo Z (2013) J Chil Chem Soc 58:2011–2015
50. Chen J, Cai H, Zhao T (2022) Mol Catal 528:112518
51. Lapin N, D'yankova NY (2013) Inorg Mater 49:975–979
52. Kalidindi SB, Indirani M, Jagirdar BR (2008) Inorg Chem 47:7424–7429
53. Wu H, Cheng Y, Fan Y, Lu X, Li L, Liu B, Li B, Lu S (2020) Int J Hydrog Energy 45:30325–30340
54. Gil-San-Millan R, Grau-Atienza A, Johnson DT, Rico-Francés S, Serrano E, Linares N, García-Martínez J (2018) Int J Hydrog Energy 43:17100–17111
55. Gangal AC, Edla R, Iyer K, Biniwale R, Vashistha M, Sharma P (2012) Int J Hydrog Energy 37:3712–3718
56. Chandra M, Xu Q (2006) J Power Sources 159:855–860
57. Brockman A, Zheng Y, Gore J (2010) Int J Hydrog Energy 35:7350–7356
58. Wang WH, Tang HP, Lu WD, Li Y, Bao M, Himeda Y (2017) ChemCatChem 9:3191–3196
59. Faverio C, Boselli MF, Medici F, Benaglia M (2020) Org Biomol Chem 18:7789–7813
60. Chandra M, Xu Q (2007) J Power Sources 168:135–142
61. Zahmakıran M, Durap F, Özkar S (2010) Int J Hydrog Energy 35:187–197
62. Xu Q, Chandra M (2006) J Power Sources 163:364–370
63. Yan J-M, Zhang X-B, Han S, Shioyama H, Xu Q (2009) Inorg Chem 48:7389–7393
64. Yan JM, Zhang XB, Han S, Shioyama H, Xu Q (2008) Angew Chem Int Ed 47:2287–2289

65. Kelly HC, Marriott VB (1979) Inorg Chem 18:2875–2878
66. Zahmakıran M, Özkar S (2009) Appl Catal B 89:104–110